Inorg. Chem. **2005**, *44*, 206–216

High-Frequency, High-Field EPR; Magnetic Susceptibility; and X-ray Studies on a Ferromagnetic Heterometallic Complex of Diethanolamine (H_2L), $[Cu_4(NH_3)_4(HL)_4][CdBr_4]Br_2 \cdot 3dmf \cdot H_2O$

Elena A. Buvaylo,[†] Vladimir N. Kokozay,[†] Olga Yu. Vassilyeva,[†] Brian W. Skelton,[‡] Julia Jezierska,[§] Louis C. Brunel,[||] and Andrew Ozarowski*,[||]

Department of Inorganic Chemistry, National Taras Shevchenko University, Volodimirska str. 64, Kyiv 01033, Ukraine, Chemistry, School of Biomedical and Chemical Sciences, University of Western Australia, Crawley, Western Australia 6009, Australia, Faculty of Chemistry, University of Wroclaw, 14 Joliot-Curie Str., 50-383 Wroclaw, Poland, and National High Magnetic Field Laboratory, Florida State University, 1800 E. Paul Dirac Drive, Tallahassee, Florida 32310

Received July 19, 2004

The novel heterometallic complex $[Cu_4(NH_3)_4(HL)_4][CdBr_4]Br_2 \cdot 3dmf \cdot H_2O$ has been prepared in the reaction of zerovalent copper with cadmium oxide in the air-exposed solution of ammonium bromide and diethanolamine (H_2L) in dimethylformamide (dmf). The compound is monoclinic, with space group $P2_1/c$, $a = 14.876(3)$ Å, $b = 33.018(6)$ Å, $c = 11.437(2)$ Å, $\beta = 108.182(3)°$, and $Z = 4$. The crystal lattice consists of $[Cu_4(NH_3)_4(HL)_4]^{4+}$ cations, $[CdBr_4]^{2-}$, Br^- anions, and uncoordinated dmf and water molecules. In the cation, four independent Cu atoms occupy vertexes of a distorted tetrahedron with bridged Cu···Cu distances in the range 3.127(2)–3.333(3) Å and other Cu···Cu separations being 3.445(3)–3.503(2) Å. The magnetic susceptibility and the EPR spectra were measured over the temperature ranges 1.8–300 and 3–300 K, respectively. The magnetic moment was found to increase with decreasing temperature to reach a maximum of 2.60 μ_B per one copper atom at ca. 10 K and was found, subsequently, to diminish slightly at lower temperatures owing to zero-field and Zeeman splitting of the $S = 2$ ground state. The temperature dependence of the magnetic susceptibility was fitted to the spin Hamiltonian $H = J_{ab}\mathbf{S}_a\mathbf{S}_b + J_{bc}\mathbf{S}_b\mathbf{S}_c + J_{cd}\mathbf{S}_c\mathbf{S}_d + J_{ad}\mathbf{S}_a\mathbf{S}_d + J_{ac}\mathbf{S}_a\mathbf{S}_c + J_{bd}\mathbf{S}_b\mathbf{S}_d$ with the exchange integrals $J_{ab} = J_{bc} = J_{cd} = J_{ad} = -65(3)$ cm^{-1} and $J_{ac} = J_{bd} = +1(3)$ cm^{-1}. High-field, high-frequency (95–380 GHz) EPR spectra due to an $S = 2$ ground state were simulated with $g_x = 2.138(1)$, $g_y = 2.142(1)$, $g_z = 2.067(1)$, $D = -0.3529(3)$ cm^{-1}, and $E = -0.0469(8)$ cm^{-1}. Calculations based on the X-ray structure indicate a negligible contribution of the magnetic dipole–dipole interactions to the zfs parameters D and E. A discussion of the isotropic and anisotropic exchange interactions and their effect on the zfs parameters is also given.

Introduction

There has been continuous interest in high-nuclearity transition-metal complexes with studies aimed at the elucidation of the magnetic exchange interactions between paramagnetic metal ions,[1] modeling of structural and functional aspects of multimetallic active sites of biological metalloenzymes,[2] and production of new nanometric materials such as molecular magnets.[3] In particular, much attention has been given to copper because of the central role it plays in biology. Multicopper compounds have also been extensively studied from a magnetostructural viewpoint because of the inherent interest in relating structure to the exchange interactions. The relatively simple case of four copper(II) ions, where the electronic spins of four copper ions are coupled to give a quintet, three triplet, and two singlet spin states, continues to draw attention because it offers opportunities to rationalize the relationship between structure and magnetic behavior in

* E-mail: ozarowsk@magnet.fsu.edu. Tel: 850-644-5996. Fax: 850-644-1366.
[†] National Taras Shevchenko University.
[‡] University of Western Australia.
[§] University of Wroclaw.
[||] Florida State University.

(1) Kahn, O. *Molecular Magnetism*; VCH: New York, 1993. Kahn, O. *Adv. Inorg. Chem.* **1995**, *43*, 179−259. Gatteschi, D. *Adv. Mater. (Weinheim, Ger.)* **1994**, *6*, 635−645. *Molecular Magnetic Materials*; Gatteschi, D., Kahn, O., Miller, J. S., Palacio, F., Eds.; NATO ASI Series; Kluwer: Dordrecht, The Netherlands, 1991.

10.1021/ic049044p CCC: $30.25
Published on Web 12/15/2004

these versatile geometric arrays of four metal atoms.[4] Historically, these are the best-understood systems, and their magnetic susceptibility can generally be explained, while successful EPR investigations are less frequent.

Pursuing our research on the use of zerovalent metals in preparations of metal complexes,[5] we report here the magnetic properties of a novel heterometallic solid built of a tetracopper cubane-type cation and perbromocadmate ($CdBr_4^{2-}$) and bromide anions that is formed serendipitously in the interaction of copper powder, cadmium oxide, ammonium bromide, and diethanolamine (H_2L) in dimethylformamide (dmf) exposed to air. Reactions employing elemental copper and amino alcohol allow in situ formation of the metal aminoalkoxo species, key building blocks that can subsequently self-assemble with other metal centers present in the reaction vessel. The subtle interactions that control the formation of complexes under such conditions and their architectural characteristics may be rationalized after the event, but they can rarely be predicted in advance.

The compound $[Cu_4(NH_3)_4(HL)_4][CdBr_4]Br_2 \cdot 3dmf \cdot H_2O$ appears to be an example of a tetranuclear system that also allows a successful EPR study. Interactions between clusters in the crystal lattice are weak so that extra complications of the magnetic behavior as well as the exchange narrowing of the EPR lines are of little concern; the exchange interactions within the cluster are ferromagnetic, making very low temperature EPR experiments possible, and of sufficient magnitude to result in a clear separation of the spin-quintet ground state from other levels. A detailed analysis of the magnetic and EPR properties is thus presented.

Experimental Section

Materials and Instrumentation. Commercially available chemicals were used as received. All experiments were carried out in air. Elemental analyses were performed by atomic absorption spectroscopy for metals and by the microanalytical service at the Faculty of Chemistry, University of Wroclaw, for carbon, hydrogen, and nitrogen. The bromide contents were determined using titration with silver nitrate (Volhard method). Infrared spectra of KBr disks were recorded on an UR-10 spectrophotometer in the 4000−400 cm^{-1} region using conventional techniques. X-band EPR spectra were recorded on a Bruker ESP 300E (Bruker, Rheinstetten, Germany) spectrometer equipped with a Bruker NMR gaussmeter ER 035M and a Hewlett-Packard microwave frequency counter HP 5350B. High-frequency EPR spectra were recorded on a home-built spectrometer at the EMR facility of NHMFL.[6] The instrument was a transmission-type device in which waves are propagated in cylindrical lightpipes. The microwaves were generated by Gunn oscillators, operating at 95 ± 3 GHz or at 110 ± 4 GHz. Frequencies higher by a factor 2, 3, or 4 were obtained using a Schottky diode-based multiplier and appropriate high-pass filters. A hot-electron bolometer cooled by liquid helium was used as a microwave detector. The field-modulated EPR signal was processed by a Stanford SR830 lock-in amplifier. The instrument used no resonance cavity. A superconducting magnet (Oxford Instruments) capable of reaching a field of 17 T was employed. The temperature was controlled with an Oxford Instruments CF1200 continuous-flow liquid-helium cryostat and an IC503 controller. Magnetic susceptibility data of a powdered sample were measured with a SQUID-based (Quantum Design) MPMSXL-5-type magnetometer over the temperature range 1.8−300 K and at a magnetic induction of 0.5 T. Magnetization data were taken at $T = 2$ K over the magnetic induction range 0.01−5.0 T. In all cases, corrections for the sample holders were applied. Diamagnetic corrections for the tetrameric molecule (733×10^{-6} cgs emu) were determined from Pascal's constants.

Preparation of $[Cu_4(NH_3)_4(HL)_4][CdBr_4]Br_2 \cdot 3dmf \cdot H_2O$. Copper powder (0.16 g, 2.5 mmol), CdO (0.32 g, 2.5 mmol), NH_4Br (0.97 g, 10 mmol), dmf (10 cm^3), and H_2L (0.5 cm^3) were heated to 50−60 °C and stirred for ca. 10 min until the total dissolution of copper was observed. The resulting blue solution was filtered and allowed to stand at room temperature. Dark-blue microcrystals of the desired compound precipitated within 1 day. They were collected by filter suction and dried in vacuo. Yield: 0.6 g, 61.2%.Anal. Calcd for $C_{25}H_{75}Br_6CdCu_4N_{11}O_{12}$ (1567.96): Cu, 16.21; Cd, 7.17; Br, 30.58; C, 19.15; H, 4.82; N, 9.83. Found: Cu, 16.1; Cd, 7.5; Br, 30.6; C, 12.0; H, 4.9; N, 9.7. The crystals appear to deteriorate with time because of solvent loss. Elemental analyses of the samples stored over extended time were consistent with the formula $[Cu_4(NH_3)_4(HL)_4][CdBr_4]Br_2 \cdot dmf$. Anal. Calcd for $C_{19}H_{59}Br_6CdCu_4N_9O_9$ (1403.75): C, 16.26; H, 4.24; N, 8.98. Found: C, 16.70; H, 4.08; N, 8.67. Found: C, 16.23; H, 4.01; N, 8.42. The best results in magnetic fittings ($g_{average}$ consistent with the EPR data) were obtained assuming that the compound lost 2% of its mass (with respect to 1567.96).

X-ray Crystallographic Investigations. The diffraction experiment was performed on a Bruker SMART CCD diffractometer (ω rotation scans with narrow frames) using graphite-monochromated Mo Kα radiation ($\lambda = 0.710\,73$ Å). The data were corrected for Lorentz polarization effects and for the effects of absorption (multiscan). The structure was solved by direct methods using

(2) Kaim, W.; Schwederski, B. *Bioinorganic Chemistry: Inorganic Elements in the Chemistry of Life*; Wiley: Chichester, U.K., 1995. Quintanar, L.; Gebhard, M.; Wang, T. P.; Kosman, D. J.; Solomon, E. I. *J. Am. Chem. Soc.* **2004**, *126*, 6579−6589. Lee, S. K.; George, S. D.; Antholine, W. E.; Hedman, B.; Hodgson, K. O.; Solomon, E. I. *J. Am. Chem. Soc.* **2002**, *124*, 6180−6193. Cole, A. P.; Root, D. E.; Mukherjee, P.; Solomon, E. I.; Stack, T. D. P. *Science* **1996**, *273*, 1848−1850. Gebbink, R. J. M. K.; Sandee, A. J.; Peters, F. G. A.; Van Der Gaast, S. J.; Feiters, M. C.; Nolte, R. J. M. *J. Chem. Soc., Dalton Trans.* **2001**, 3056−3064. Holm, R. H.; Kennepohl, P.; Solomon, E. I. *Chem. Rev.* **1996**, *96*, 2239−2314.

(3) Lippard, S. J. *Angew. Chem., Int. Ed. Engl.* **1988**, *27*, 344−361. Parsons, S.; Winpenny, R. E. P. *Acc. Chem. Res.* **1997**, *30*, 89−95. Müller, A.; Peters, F.; Pope, M. T.; Gatteschi, D. *Chem. Rev.* **1998**, *98*, 239−271. Gatteschi, D.; Sessoli, R.; Cornia, A. *Chem. Commun.* **2000**, 725−732.

(4) Ray, M. S.; Ghosh, A.; Das, A.; Drew, M. G. B.; Ribas-Ariño, J.; Novoa, J.; Ribas, J. *Chem. Commun.* **2004**, 1102−1103. Tan, X. S.; Fujii, Y.; Nukada, R.; Mikuriya, M.; Nakano, Y. *J. Chem. Soc., Dalton Trans.* **1999**, 2415−2416. Doyle, R. P.; Kruger, P. E.; Moubaraki, B.; Murray, K. S.; Nieuwenhuyzen, M. *J. Chem. Soc., Dalton Trans.* **2003**, 4230−4237. Koval, I. A.; Gamez, P.; Roubeau, O.; Driessen, W. L.; Lutz, M.; Spek, A. L.; Reedijk, J. *Inorg. Chem.* **2003**, *42*, 868−872.

(5) Kovbasyuk, L. A.; Vassilyeva, O. Yu.; Kokozay, V. N.; Linert, W.; Reedijk, J.; Skelton, B. W.; Oliver, A. G. *J. Chem. Soc., Dalton Trans.* **1998**, 2735−2738. Makhankova, V. G.; Vassilyeva, O. Yu.; Kokozay, V. N.; Skelton, B. W.; Reedijk, J.; van Albada, G. A.; Sorace, L.; Gatteschi, D. *New J. Chem.* **2001**, *25*, 685−689. Vinogradova, E. A.; Vassilyeva, O. Yu.; Kokozay, V. N.; Squattrito, P. J.; Reedijk, J.; van Albada, G. A.; Linert, W.; Tiwary, S. K.; Raithby, P. R. *New J. Chem.* **2001**, *25*, 949−953. Makhankova, V. G.; Vassilyeva, O. Yu.; Kokozay, V. N.; Skelton, B. W.; Sorace, L.; Gatteschi, D. *J. Chem. Soc., Dalton Trans.* **2002**, 4253−4259. Vinogradova, E. A.; Vassilyeva, O. Yu.; Kokozay, V. N.; Skelton, B. W.; Bjernemose, J. K.; Raithby, P. R. *J. Chem. Soc., Dalton Trans.* **2002**, 4248−4252. Vinogradova, E. A.; Kokozay, V. N.; Vassilyeva, O. Yu.; Skelton, B. W. *Inorg. Chem. Commun.* **2003**, *6*, 82−85.

(6) Hassan, A. K.; Pardi, L. A.; Krzystek, J.; Sienkiewicz, A.; Goy, P.; Rohrer, M.; Brunel, L.-C. *J. Magn. Reson.* **2000**, *142*, 300−312.

Table 1. Crystallographic Data and Relevant Data Referring to the Structure Solution and Refinement

empirical formula	$C_{25}H_{75}Br_6CdCu_4N_{11}O_{12}$
formula weight	1567.96
crystal system	monoclinic
space group	$P2_1/c$
a [Å]	14.876(3)
b [Å]	33.018(6)
c [Å]	11.437(2)
β [deg]	108.182(3)
V [Å^3]	5337.1(17)
Z	4
μ [mm^{-1}]	6.508
measured reflections	41 117
observed reflections	8148
R_{int}	0.059
R	0.068
wR	0.123

XTAL3.7.[7] Details of the structural investigation and crystallographic data are summarized in Table 1.

The non-hydrogen atoms were refined anisotropically (full-matrix least squares). Part of the cation is disordered over two sites; these are the atoms C(6), C(7), C(8), O(4), and N(2) of one HL; the copper atom to which they are coordinated, Cu(3); and the ammonia nitrogen atom N(6), which is bound to Cu(3). Thus, each of these atoms has primed and unprimed components. In sympathy with this, the bromide ion Br(2) and the water molecule O(9) are also disordered and have primed and unprimed components. The hydrogen atoms for O(9) and O(9′) were not located. From initial trial refinement of the site occupancy factors, these disordered atoms were each assigned an occupancy of 0.5. The $CdBr_4^{2-}$ anion is also disordered; the two sets of sites for Br(12)−Br(14) have site occupancies of 0.866(2) and 1-0.866(2). Br(11) is common to both components. The dmf molecule [O(03)] is disordered, with site occupancy factors of the two sets of components of the carbonyl carbon [C(03) and C(03′)] and the Me groups [C(031), C(032) and C(031′), C(032′)] being refined to 0.72(2) and 1-0.72(2). The oxygen and nitrogen atoms [O(03) and N(03)] are common to both components. It seems that this disorder is not dependent on the disorder in the cation; there are no close contacts between the two, and the site occupancies were refined to different values. The geometries involving the minor component of the disordered dmf and the disordered atoms of the HL were restrained to ideal values in the refinement.

Results

Synthesis and Spectroscopic Characterization. The reaction of copper powder with CdO, H_2L, and ammonium bromide in a nonaqueous solvent in open air using a molar ratio of Cu:MO:H_2L:NH_4Br = 1:1:2:4 gave a compound that showed the stoichiometry Cu:Cd:Br = 4:1:4. The ratio of metals in the reaction mixture did not appear to affect the nature of the reaction product. In the process, dioxygen was reduced to give H_2O and Cu^0 was oxidized to Cu(II). The overall reaction is

$$4Cu^0 + CdO + 6NH_4Br + 4H_2L + 2O_2 + 3dmf \rightarrow [Cu_4(NH_3)_4(HL)_4][CdBr_4]Br_2\cdot 3dmf\cdot H_2O + 2NH_3 + 4H_2O \quad (1)$$

The single-crystal X-ray structural analysis (see below) conclusively proved the identity of the complex as $[Cu_4(NH_3)_4(HL)_4][CdBr_4]Br_2\cdot 3dmf\cdot H_2O$.

The IR spectrum in the range 4000−400 cm^{-1} shows characteristic ligand peaks, indicating the presence of hydrogen-bonded OH groups (3400−3500 cm^{-1}). A distinctive band at 1260 cm^{-1} is assigned to N−H stretching of the NH_3 molecules. An intense band corresponding to ν(CO) vibrations of dmf was clearly observed at 1600 cm^{-1}.

Molecular and Crystal Structure. The compound is built of the tetranuclear cation $[Cu_4(NH_3)_4(HL)_4]^{4+}$, $[CdBr_4]^{2-}$ and Br^- anions, and uncoordinated dmf and water molecules. Each copper center is coordinated by two alkoxo oxygen atoms, one amine nitrogen atom of the monodeprotonated HL ligands, and one nitrogen atom from the ammonia molecule. That geometry is square-planar with the Cu−O and Cu−N bond lengths in the range 1.928(7)−2.099(7) Å (Table 2 and Figure 1). In addition, copper atoms are weakly bonded to the ethanol group of the chelating HL ligand and an alkoxo oxygen atom from a neighboring HL ligand [Cu−O = 2.421(7)−2.692(7) Å], which implies that the metal-coordination sphere approximates an elongated octahedron. Each HL ligand adopts a chelating−bridging mode, forming five-membered rings with the ethanol group weakly coordinated, a coordination mode that is common for dinuclear copper complexes of this ligand.[8] However, in the structure under discussion, the alkoxo oxygen atoms bridge three copper atoms rather than two: each of the oxygen atoms O1, O3, O5, and O7, besides being bound to two copper atoms, are also weakly coordinated to a third copper atom (Cu4, Cu2, Cu3, and Cu1, respectively; Figure 2). This bridging mode results in the formation of a Cu_4O_4 cluster that is made up of a copper tetrahedron interlocked with an oxygen tetrahedron and that is closely related to the cubane-type structures. Distances between the oxygen-bridged copper atoms lie in the range 3.127(2)−3.333(3) Å, while other Cu···Cu separations are 3.445(3)−3.503(2) Å (Table 2). The $[CdBr_4]^{2-}$ anion is structurally normal, with the Cd−Br distances for the major component falling in the range 2.563(2)−2.584(2) Å and the Br−Cd−Br angles of 106.04(5)−112.98(6)° showing minor distortions of the $CdBr_4$ tetrahedron.

The crystal lattice is stabilized by strong hydrogen bonds between the OH and NH groups of the ligands and solvent molecules with distances that vary from 2.49(2) to 2.99(2) Å and between the OH and uncoordinated $CdBr_4^{2-}$ anions with distances in the range 3.08(2)−3.39(2) Å. Further details of the hydrogen bonds are included in Table 3.

Magnetic Properties of $[Cu_4(NH_3)_4(HL)_4][CdBr_4]Br_2\cdot 3dmf\cdot H_2O$. The magnetic moment (Figure 3) increases with decreasing temperature, reaching a maximum of 2.60 μ_B per one copper atom at ca. 10 K, and subsequently diminishes slightly at the lowest temperatures. Interestingly, a closely related compound, chloro(2-diethylaminoethanolato)copper(II) tetramer, exhibits very different magnetic behavior,[9] with

(7) *XTAL3.7 System*; Hall, S. R., du Boulay, D. J., Olthof-Hazekamp, R., Eds.; University of Western Australia: Crawley, Australia, 2000.

(8) Karadag, A.; Yilmaz, V. T.; Thoene, C. *Polyhedron* **2001**, *20*, 635−641. Madarász, J.; Bombicz, P.; Czugler, M.; Pokol, G. *Polyhedron* **2000**, *19*, 457−463. Yilmaz, V. T.; Topcu, Y.; Yilmaz, F.; Thoene, C. *Polyhedron* **2001**, *20*, 3209−3217.

Table 2. Selected Bond Distances (Å) and Angles (deg)

Cd(1)−Br(11)	2.5844(15)	Cu(3)−O(1)	1.928(7)
Cd(1)−Br(12)	2.5828(15)	Cu(3)−O(3)	1.806(7)
Cd(1)−Br(13)	2.5807(15)	Cu(3)−O(4)	2.487(17)
Cd(1)−Br(14)	2.5633(19)	Cu(3)−O(5)	2.692(7)
Cd(1)−Br(12′)	2.529(12)	Cu(3)−N(2)	2.072(15)
Cd(1)−Br(13′)	2.529(10)	Cu(3)−N(6)	1.999(13)
Cd(1)−Br(14′)	2.747(9)	Cu(3′)−O(1)	2.057(8)
Cu(1)−O(1)	1.955(8)	Cu(3′)−O(3)	2.099(7)
Cu(1)−O(2)	2.606(7)	Cu(3′)−O(4′)	2.528(14)
Cu(1)−O(5)	1.969(7)	Cu(3′)−O(5)	2.421(7)
Cu(1)−O(7)	2.512(6)	Cu(3′)−N(2′)	2.012(15)
Cu(1)−N(1)	2.038(9)	Cu(3′)−N(6′)	2.007(15)
Cu(1)−N(5)	1.990(9)	Cu(4)−O(1)	2.485(7)
Cu(2)−O(3)	2.543(7)	Cu(4)−O(3)	1.973(8)
Cu(2)−O(5)	1.935(6)	Cu(4)−O(7)	1.957(7)
Cu(2)−O(6)	2.571(8)	Cu(4)−O(8)	2.532(8)
Cu(2)−O(7)	1.960(7)	Cu(4)−N(4)	2.024(9)
Cu(2)−N(3)	2.045(9)	Cu(4)−N(8)	2.010(14)
Cu(2)−N(7)	2.025(9)		
Cu(1)···Cu(2)	3.158(2)	Cu(1)···Cu(4)	3.445(3)
Cu(1)···Cu(3)	3.249(2)	Cu(2)···Cu(3)	3.503(2)
Cu(1)···Cu(3′)	3.127(2)	Cu(2)···Cu(3′)	3.455(2)
Cu(2)···Cu(4)	3.173(2)		
Cu(3)···Cu(4)	2.974(3)		
Cu(3′)···Cu(4)	3.333(3)		
Br(11)−Cd−Br(12)	112.98(6)	O(1)−Cu(3)−O(4)	95.0(4)
Br(11)−Cd−Br(13)	106.04(5)	O(1)−Cu(3)−O(5)	70.3(3)
Br(11)−Cd−Br(14)	108.28(6)	O(1)−Cu(3)−N(2)	171.6(5)
Br(11)−Cd−Br(12′)	114.7(3)	O(1)−Cu(3)−N(6)	89.7(5)
Br(11)−Cd−Br(13′)	121.1(2)	O(3)−Cu(3)−O(4)	101.8(4)
Br(11)−Cd−Br(14′)	95.24(16)	O(3)−Cu(3)−O(5)	77.4(3)
Br(12)−Cd−Br(13)	110.57(5)	O(3)−Cu(3)−N(2)	82.2(4)
Br(12)−Cd−Br(14)	106.38(5)	O(3)−Cu(3)−N(6)	164.6(6)
Br(12)−Cd−Br(13′)	110.7(2)	O(4)−Cu(3)−O(5)	165.1(4)
Br(13)−Cd−Br(14)	112.67(6)	O(4)−Cu(3)−N(2)	79.1(6)
Br(12′)−Cd−Br(13′)	108.9(3)	O(4)−Cu(3)−N(6)	93.0(6)
Br(12′)−Cd−Br(14′)	109.5(3)	O(5)−Cu(3)−N(2)	115.2(5)
Br(13′)−Cd−Br(14′)	105.6(3)	O(5)−Cu(3)−N(6)	89.4(5)
O(1)−Cu(1)−O(2)	91.8(3)	N(2)−Cu(3)−N(6)	96.6(6)
O(1)−Cu(1)−O(5)	88.2(3)	O(1)−Cu(3′)−O(3)	81.5(3)
O(1)−Cu(1)−O(7)	78.8(2)	O(1)−Cu(3′)−O(4′)	89.4(4)
O(1)−Cu(1)−N(1)	84.6(3)	O(1)−Cu(3′)−O(5)	74.7(3)
O(1)−Cu(1)−N(5)	171.2(3)	O(1)−Cu(3′)−N(2′)	164.2(5)
O(2)−Cu(1)−O(5)	97.4(3)	O(1)−Cu(3′)−N(6′)	98.0(5)
O(2)−Cu(1)−O(7)	166.6(2)	O(3)−Cu(3′)−O(4′)	93.4(3)
O(2)−Cu(1)−N(1)	75.6(3)	O(3)−Cu(3′)−O(5)	79.3(2)
O(2)−Cu(1)−N(5)	96.5(3)	O(3)−Cu(3′)−N(2′)	87.5(4)
O(5)−Cu(1)−O(7)	73.0(2)	O(3)−Cu(3′)−N(6′)	173.4(5)
O(5)−Cu(1)−N(1)	169.8(3)	O(4′)−Cu(3′)−O(5)	163.3(3)
O(5)−Cu(1)−N(5)	93.6(3)	O(4′)−Cu(3′)−N(2′)	79.8(6)
O(7)−Cu(1)−N(1)	112.5(3)	O(4′)−Cu(3′)−N(6′)	93.2(5)
O(7)−Cu(1)−N(5)	93.5(3)	O(5)−Cu(3′)−N(2′)	114.6(5)
N(1)−Cu(1)−N(5)	94.6(4)	O(5)−Cu(3′)−N(6′)	94.2(5)
O(3)−Cu(2)−O(5)	79.3(3)	N(2′)−Cu(3′)−N(6′)	94.2(6)
O(3)−Cu(2)−O(6)	164.2(2)	O(1)−Cu(4)−O(3)	74.0(3)
O(3)−Cu(2)−O(7)	73.4(3)	O(1)−Cu(4)−O(7)	79.4(2)
O(3)−Cu(2)−N(3)	115.2(3)	O(1)−Cu(4)−O(8)	166.3(3)
O(3)−Cu(2)−N(7)	93.8(4)	O(1)−Cu(4)−N(4)	114.0(3)
O(5)−Cu(2)−O(6)	92.0(2)	O(1)−Cu(4)−N(8)	91.4(4)
O(5)−Cu(2)−O(7)	87.8(3)	O(3)−Cu(4)−O(7)	88.0(3)
O(5)−Cu(2)−N(3)	85.6(3)	O(3)−Cu(4)−O(8)	93.1(3)
O(5)−Cu(2)−N(7)	172.0(4)	O(3)−Cu(4)−N(4)	168.7(3)
O(6)−Cu(2)−O(7)	93.2(3)	O(3)−Cu(4)−N(8)	94.7(4)
O(6)−Cu(2)−N(3)	76.9(3)	O(7)−Cu(4)−O(8)	95.9(3)
O(6)−Cu(2)−N(7)	95.6(4)	O(7)−Cu(4)−N(4)	85.7(4)
O(7)−Cu(2)−N(3)	167.9(3)	O(7)−Cu(4)−N(8)	169.3(4)
O(7)−Cu(2)−N(7)	94.0(4)	O(8)−Cu(4)−N(4)	78.2(3)
N(3)−Cu(2)−N(7)	93.8(4)	O(8)−Cu(4)−N(8)	94.3(4)
O(1)−Cu(3)−O(3)	93.2(3)	N(4)−Cu(4)−N(8)	93.2(5)

the magnetic moment decreasing as the temperature is lowered over the range 70−7 K.

(9) Hall, J. W.; Estes, W. E.; Estes, E. D.; Scaringe, R. P.; Hatfield, W. E. *Inorg. Chem.* **1977**, *16*, 1572−1574.

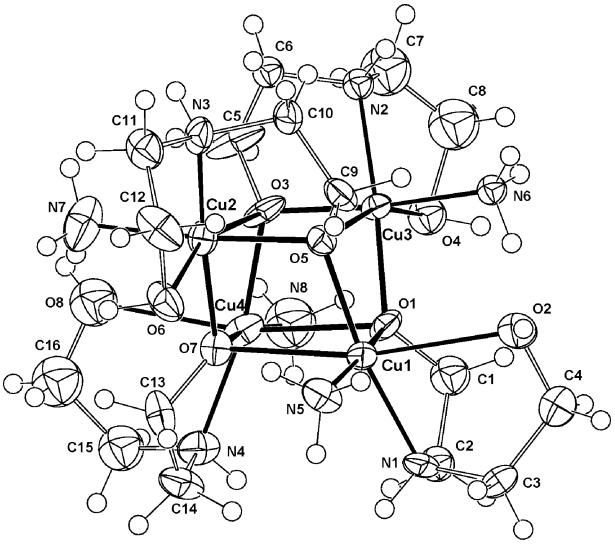

Figure 1. Molecular structure of the tetranuclear cation in $[Cu_4(NH_3)_4(HL)_4][CdBr_4]Br_2 \cdot 3dmf \cdot H_2O$ (unprimed component only) with 50% displacement ellipsoids and the atom-numbering scheme. Hydrogen atoms are drawn as spheres of an arbitrary radius.

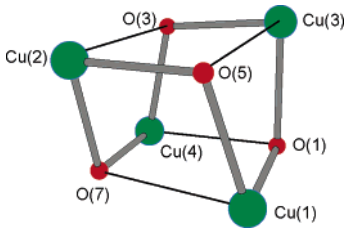

Figure 2. Structure of the Cu_4O_4 core in $[Cu_4(NH_3)_4(HL)_4][CdBr_4]Br_2 \cdot 3dmf \cdot H_2O$. Each of the oxygen atoms forms strong bonds to two neighboring copper atoms (thick lines) and a weaker bond to a third copper atom (thin lines).

Table 3. Hydrogen-Bonding Geometry (Å, deg)[a]

D−H···A	H···A	D···A	D−H···A
N(2)−H(2N)···Br(2[1])	2.46	3.39(2)	164
N(3)−H(3N)···Br(2[2])	2.42	3.248(9)	148
N(4)−H(4N)···O(01)	1.98	2.84(1)	157
N(5)−H(5bN)···O(6)	2.03	2.94(1)	168
N(6′)−H(6′aN)···O(2)	2.05	2.87(2)	147
N(7)−H(7cN)···O(9)	1.88	2.79(2)	162
N(8)−H(8bN)···O(4)	1.88	2.78(2)	158
N(8)−H(8aN)···O(01)	2.17	2.99(2)	150
O(2)−H(2O)···Br(1)	2.31	3.22(1)	158
O(4)−H(4O)···Br(11)	2.75	3.17(2)	111
O(6)−H(6O)···O(02)	1.79	2.63(1)	149
O(8)−H(8O)···O(9)	2.42	2.92(2)	113
O(9)···O(03)		2.49(2)	
O(9)···Br(2)		3.08(2)	

[a] Symmetry operations: [1]$x, y, 1 + z$; [2]$1 - x, 1 - y, 1 - z$.

The exchange interaction within a tetrameric molecule can be described by the Hamiltonian[10,11]

$$H = J_{ab}\mathbf{S}_a\mathbf{S}_b + J_{bc}\mathbf{S}_b\mathbf{S}_c + J_{cd}\mathbf{S}_c\mathbf{S}_d + J_{ad}\mathbf{S}_a\mathbf{S}_d + J_{ac}\mathbf{S}_a\mathbf{S}_c + J_{bd}\mathbf{S}_b\mathbf{S}_d \quad (2)$$

The Hamiltonian gives rise to six eigenstates of the total spin operator $\mathbf{S} = \mathbf{S}_a + \mathbf{S}_b + \mathbf{S}_c + \mathbf{S}_d$: two singlets ($S = 0$),

(10) Sinn, E. *Coord. Chem. Rev.* **1970**, *5*, 313−347.
(11) Bencini, A.; Gatteschi, D. *EPR of Exchange Coupled Systems*; Springer-Verlag: Berlin, Germany, 1990.

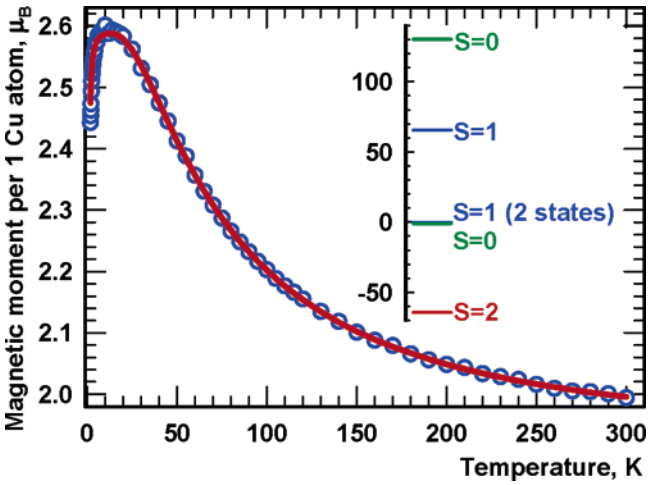

Figure 3. Plot of the magnetic moment per one copper atom versus temperature. The solid line was calculated based on eqs 8−10 with $J_{ab} = J_{bc} = J_{cd} = J_{ad} = -65$ cm^{-1}, $J_{ac} = J_{bd} = 1$ cm^{-1}, $g_{x,y} = 2.14$, $g_z = 2.067$, $D = -0.353$ cm^{-1}, and $E = -0.047$ cm^{-1}. Calculated spin-state energies (in cm^{-1}) are shown in the inset.

three triplets ($S = 1$), and one quintet state ($S = 2$). Their relative energies, which determine the magnetic properties, depend on relations between particular J values. The formulas for the energies resulting from the Hamiltonian (eq 2) that have been given in many papers[10,11] usually assume some degree of symmetry so that certain exchange integrals are equal. Analytical formulas for the most general case (all J values being different) can be derived. A convenient set of formulas is obtained by introducing the symbols

$$a = (J_{ab} + J_{cd})/4, \quad b = (J_{ac} + J_{bd})/4, \quad c = (J_{bc} + J_{ad})/4,$$
$$d = (J_{ab} - J_{cd})/4, \quad e = (J_{ac} - J_{bd})/4,$$
$$f = (J_{bc} - J_{ad})/4 \quad (3)$$

With these symbols, the quintet-state energy is

$$E_Q = a + b + c \quad (4)$$

while the singlet- and triplet-state energies are calculated by solving quadratic and cubic equations, respectively, resulting from the following secular determinants:

Singlet states

$$\begin{vmatrix} a - 2b - 2c - E_S & \sqrt{3}(c - b) \\ \sqrt{3}(c - b) & -3a - E_S \end{vmatrix} = 0 \quad (5)$$

Triplet states

$$\begin{vmatrix} -a - b + c - E_T & 2d & 2e \\ 2d & -a + b - c - E_T & 2f \\ 2e & 2f & a - b - c - E_T \end{vmatrix} = 0 \quad (6)$$

The convenience of these formulas lies in the fact that, in the presence of symmetry within a tetrameric molecule, like $J_{ab} = J_{cd}$, one or more of the quantities d, e, and f are equal to 0, resulting in further factorization of the secular equations. Energies calculated from the above formulas, in special cases, fully agree with those given in refs 10 and 11.

The magnetic susceptibility per $^1/_4$ of the molecular mass can be calculated from

$$\chi = \frac{N\mu_B{}^2 g^2}{12kT} \frac{\sum_{i=1}^{6}(2S_i + 1)(S_i + 1)S_i \exp(-E_i/kT)}{\sum_{i=1}^{6}(2S_i + 1)\exp(-E_i/kT)} \quad (7)$$

In the heterocycle Cu_4O_4, all Cu−O−Cu bond angles are of very similar magnitudes of about 107°. Assuming the sequence a−b−c−d of the copper atoms in the ring, we may expect that the exchange interactions a−b, b−c, c−d, and d−a are of similar magnitudes, while the interactions a−c and b−d should be different and possibly smaller than those in the former group. Attempts to fit the magnetic moments with the above model were successful above ~15 K, leading to an exchange integral value of −69 cm^{-1} for a−b, b−c, c−d, and a−d and close to 0 for a−c and b−d. However, within the model, it is not possible to explain the magnetic moment lowering that occurs below 10 K. The magnitude of $\mu = 2.60\ \mu_B$ at 10 K indicates that 100% of the molecules are already in the $S = 2$ state. This is confirmed by the high-frequency EPR spectra (see below) in that only the quintet state is present. With the magnetic moment this high, the $S = 2$ must be the ground state and a plateau should be observed at temperatures lower than 10 K. It is obvious that the zero-field (zfs) and Zeeman splittings are responsible for the observed effect. Thus, we calculated the magnetic susceptibility of the $S = 2$ state from the basic principles (see, for example, ref 10):

$$\chi_{S=2} = -\frac{N}{4B} \frac{\sum_{i=1}^{5} \frac{\partial E_i}{\partial B} \exp(-E_i/kT)}{\sum_{i=1}^{5} \exp(-E_i/kT)} \quad (8)$$

where E_i are the energies of the five states, with $M_S = -2$, −1, 0, 1, and 2 within the quintet. The factor 4 in the denominator appears because the susceptibility is related to one copper atom, while the $S = 2$ system is based on four copper atoms. The M_S energies were calculated by using D, E, and g components and $B_4{}^i$ values of the spin Hamiltonian (eq 11) as found from EPR (see below). The derivatives of each energy with respect to the magnetic field were found by evaluating energies at two magnetic fields, 1 G below and 1 G above the working $B = 5000$ G of the SQUID magnetometer. The susceptibility was calculated at many orientations of the molecule versus the magnetic field and was averaged in the same way that powder EPR spectra are usually simulated; that is, it was numerically integrated with $\sin\Theta\, d\Theta\, d\Phi$. The importance of the quintet-state splitting is also illustrated by the magnetic field dependence of the effective magnetic moment measured at 2.0 K (Figure 4). There is no need to treat the $S = 1$ states in that way because the effect is important only at the lowest temperatures, at which point these states are not populated. Also, we do not

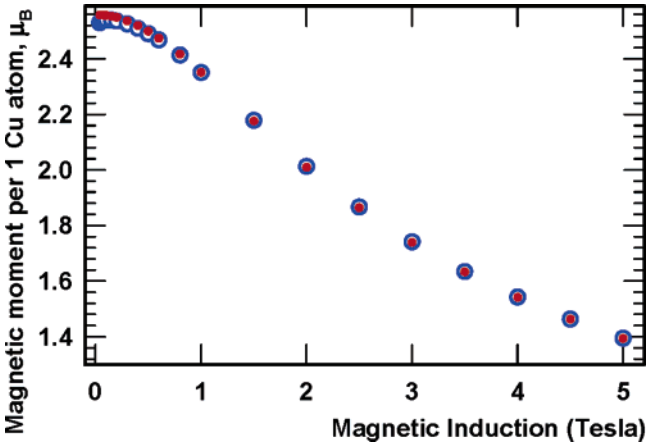

Figure 4. Effective magnetic moment at 2.0 K as a function of magnetic induction: experimental (circles) and calculated from eq 8 (dots), assuming that only the $S = 2$ state is populated.

know D and E for the triplets because they were not observed in EPR (see also the Discussion section). The magnetic susceptibility per one copper that is due to each of the triplet states was thus calculated from the well-known relation (note the factor 4 in the denominator)

$$\chi_S = (Ng^2\mu_B{}^2/3kT)S(S+1)/4 \qquad (9)$$

The final equation used for the fitting was (with $\chi_{S=2}$ calculated from eq 8 and $\chi_{S=1}$ calculated from eq 9)

$$\chi = \frac{\sum_{i=1}^{6}(2S_i+1)\chi_{S_i}\exp(-E_i/kT)}{\sum_{i=1}^{6}(2S_i+1)\exp(-E_i/kT)} + \mathrm{TIP} \qquad (10)$$

where the summation runs over all six spin states in the tetranuclear system. The fitted quantity was the product χT. In the fitting procedure, only the exchange integrals and temperature-independent paramagnetism (TIP) were allowed to vary. All other parameters (D, E, quartic terms, and g components) were fixed as found from EPR. The fitting program imposed the following constraints on the exchange integrals: $J_{ab} = J_{cd} = J_1$ and $J_{ad} = J_{bc} = J_2$ (the sequence of copper atoms in the ring is assumed to be a−b−c−d). The program consistently found $J_1 \approx J_2$ as well as $J_{ac} \approx J_{bd}$, although it was not constrained to do so. The procedure gave a very satisfactory agreement between the experimental and calculated magnetic moments (Figures 3 and 4) and led to the determination of the exchange integrals, $J_{ab} = J_{bc} = J_{cd} = J_{ad} = -65(3)$ cm^{-1} for the four pairs of bridged copper atoms and $J_{ac} = J_{bd} = +1(3)$ cm^{-1} for the two pairs of nonbridged copper atoms. The errors in the last significant digit, shown in parentheses, were estimated by using the Hessian matrix method.[12] The calculated TIP magnitude of 42×10^{-6} cgs emu (53×10^{-10} m^3/mol in SI units) is very reasonable for copper(II) and confirms the high quality of both the experimental data and the fitting procedure. Magnetic moment lowering at the lowest temperatures was observed in ferromagnetic copper tetramers previously[13,14] and was interpreted as a result of the intermolecular exchange interactions while the effect of the quintet-state splitting was not considered. The magnetic moment quenching between 10 and 4.2 K[13] and between 10 and 1.8 K[14] is stronger than that observed in our work and cannot be attributed entirely to the splitting of the $S = 2$ state, although the splitting may be of particular importance in ref 13, where the magnetic susceptibility was measured at 1 T. (No information of the magnetic field strength was given in ref 14.) The tetramer studied in this work appears to be unique in that the intermolecular interactions seem to be negligible, which can be judged from the fact that the temperature dependence of the magnetic moment is very well reproduced at all temperatures without invoking intermolecular exchange. The magnetic moment in a tetranuclear copper complex of substituted picolinic hydrazone is reported[15] to increase from room temperature down to 2 K without exhibiting a maximum, apparently because the ferromagnetic exchange is by 1 order of magnitude smaller than that in our case and states other than $S = 2$ are populated even at the lowest temperatures. The unrealistically high value of 2.246 for $g_{average}$ in ref 15 emphasizes the dangers of determining g from magnetic susceptibility data. Lowering of the magnetic moment at the lowest temperatures owing to the zfs of the ground state was also observed in other systems.[16a,b]

EPR Spectra of $[Cu_4(NH_3)_4(HL)_4][CdBr_4]Br_2\cdot 3dmf\cdot H_2O$. The powder X-band EPR spectra (Figure 5) are noninterpretable because only a part of the possible resonances can be seen, as a result of the zfs being too large compared to the microwave quantum energy. High-field spectra, taken at several frequencies between 95 and 380 GHz and at the temperature 15 K (Figure 5), enabled us to determine that the only spin state observed was the quintet, $S = 2$. No resonances that could be attributed to the triplet states were observed in EPR spectra taken over the temperature range 3−300 K (see also the Discussion section below and Figure S1 in the Supporting Information). Spectra quality deteriorated substantially at higher temperatures, while at the lowest temperatures, certain resonances were "freezed out" when both M_S levels involved in these transitions were depopulated. The latter problem becomes more serious at higher magnetic fields and higher microwave frequencies.[16a−c] A temperature of 15 K offered a reasonable compromise with good spectra quality and a majority of resonances still visible.

(12) Press, W. H.; Flannery, B. P.; Teukolsky, S. A.; Vetterling, W. T. *Numerical Recipes in Pascal*; Cambridge University Press: Cambridge, U.K., 1989.

(13) Laurent, J. P.; Bonnet, J. J.; Nepveu, F.; Astheimer, H.; Walz, L.; Haase, W. *J. Chem. Soc., Dalton Trans.* **1982**, 2433−2438.

(14) Dickinson, R. C.; Helm., F. T.; Baker, W. A.; Black, T. D.; Watson, W. H. *Inorg. Chem.* **1977**, *16*, 1530−1537.

(15) Xu, Z. Q.; Thompson, L. K.; Miller, D. O. *J. Chem. Soc., Dalton Trans.* **2002**, 2462−2466.

(16) (a) Barra, A. L.; Bencini, F.; Caneschi, A.; Gatteschi, D.; Paulsen, C.; Sangregorio, C.; Sessoli, R.; Sorace, L. *ChemPhysChem* **2001**, *2*, 523−531. (b) Ozarowski, A.; Zvyagin, S. A.; Reiff, W. M.; Telser, J.; Brunel, L. C.; Krzystek, J. *J. Am. Chem. Soc.* **2004**, *126*, 6574−6575. (c) Krzystek, J.; Zvyagin, S. A.; Ozarowski, A.; Fiedler, A. T.; Brunold, T. C.; Telser, J. *J. Am. Chem. Soc.* **2004**, *126*, 2148−2155.

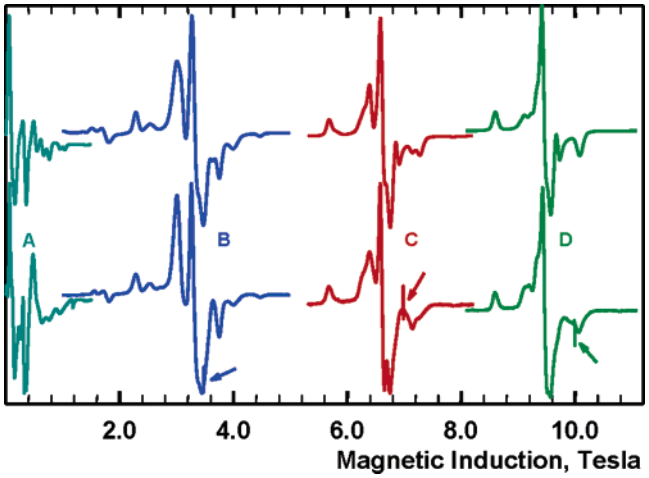

Figure 5. High-frequency and X-band EPR spectra of $[Cu_4(NH_3)_4(HL)_4][CdBr_4]Br_2 \cdot 3dmf \cdot H_2O$ at 15.0 K. A: 9.392 GHz. B: 97.675 GHz. C: 195.870 GHz. D: 280.341 GHz. Upper traces are simulated with $g_x = 2.138$, $g_y = 2.142$, $g_z = 2.067$, $D = -0.3529$ cm^{-1}, $E = -0.0469$ cm^{-1}, $B_4^0 = 0.8 \times 10^{-4}$ cm^{-1}, $B_4^2 = 2 \times 10^{-4}$ cm^{-1}, and $B_4^4 = 5 \times 10^{-4}$ cm^{-1}. Sharp resonances of DPPH used for magnetic field calibration ($g = 2.0037$) are indicated by arrows in the three high-frequency spectra.

The spin Hamiltonian appropriate for $S = 2$ is[17,18]

$$H = \mu_B \mathbf{BgS} + D\{\mathbf{S}_z^2 - (^1/_3)S(S+1)\} + E(\mathbf{S}_x^2 - \mathbf{S}_y^2) + B_4^0\mathbf{O}_4^0 + B_4^2\mathbf{O}_4^2 + B_4^4\mathbf{O}_4^4 \quad (11)$$

The spin operators $\mathbf{O}_4^i$ as well as their matrix elements can be found, for example, in ref 18. By using our own program, we were able to extract the g component and zfs parameter values by simultaneous fitting of the resonances observed at all frequencies rather than by fitting a particular spectrum. High-field EPR spectra often show artifacts caused by the poorly determined microwave modes in an instrument employing no resonance cavity and by magnetic torquing effects. The former activates resonances that are forbidden by selection rules, while the latter sometimes gives a single-crystal-like appearance to the powder spectra, making simulation of powder spectra difficult. Although both kinds of problems were not strongly pronounced in the present case, we obtained a two-dimensional dataset of the resonant fields versus microwave frequency, similar to our earlier papers.[16b,c] All resonances corresponding to the X, Y, and Z turning points in all powder spectra were treated as one dataset (Figure 6). Only very few off-axial turning points were identified in the spectra because the zfs is relatively small compared to the Zeeman splitting at the high magnetic fields used. The fitting program minimized the quantity

$$\chi^2 = \sum_{i=1}^{N}(B_i^{exp} - B_i^{calc})^2$$

where the B_i values are the experimental and calculated resonance fields (note that there are several resonance fields at each microwave frequency) and N is the total number of resonance fields fitted. An additional advantage of this numerical analysis is that the errors in the fitted parameters can be rigorously estimated by using the Hessian matrix method (p 572 in ref 12). The fitting program used the well-known Simplex algorithm (p 326 in ref 12). Calculation of the resonance fields for $S = 2$ requires diagonalization of complex 5×5 matrices, which was accomplished by using the Householder method.[19] Both the fitting program and the EPR powder simulation program used a brute-force approach without applying any simplifications. In powder simulations, the transition probabilities were evaluated from the eigenvectors. Spectra were calculated at many orientations of a molecule with respect to the magnetic field defined by the polar angles Θ and Φ and were numerically integrated with $\sin\Theta\, d\Theta\, d\Phi$ to obtain the powder EPR patterns. The fitting procedure resulted in the spin Hamiltonian parameters

$$g_x = 2.138(1), \quad g_y = 2.142(1), \quad g_z = 2.067(1),$$
$$D = -0.3529(3)\ \text{cm}^{-1}, \quad E = -0.0469(8)\ \text{cm}^{-1},$$
$$B_4^0 = 0.8(2) \times 10^{-4}, \quad B_4^2 = 2(2) \times 10^{-4},$$
$$B_4^4 = 5(2) \times 10^{-4}\ \text{cm}^{-1}$$

Individual powder spectra are nicely simulated with these parameters (Figures 5 and 7). Minor problems seen in the simulations may arise from the high-field EPR artifacts, as explained above, as well as from the fact that the structure is disordered, and we may see two species with slightly different EPR properties. It is also possible that the zfs tensor is not exactly coaxial with the **g** tensor. The fine structure

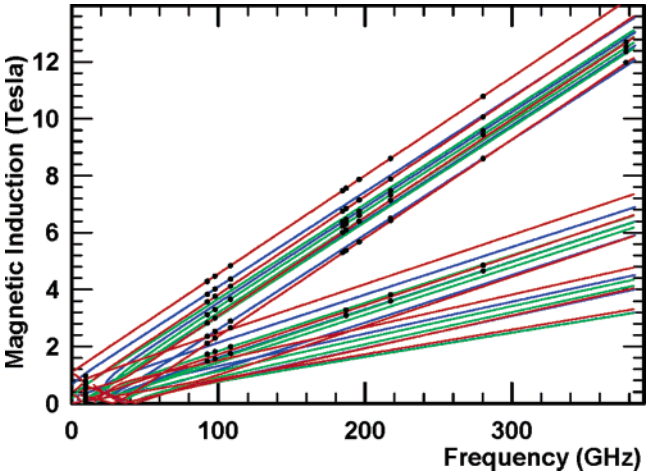

Figure 6. Experimental resonances observed in the 15.0 K EPR spectra taken at various frequencies (black dots) and calculated resonances corresponding to the X, Y, and Z orientations (green, blue, and red lines, respectively). Lines with the largest slope represent the resonances of the $\Delta M_S = 1$ type, while other branches represent transitions with $\Delta M_S = 2-4$. Resonances in the $\Delta M_S = 1$ branch can easily be correlated to those labeled in Figure 7. With B parallel to Z, the highest-field transition is $|1\rangle \rightarrow |2\rangle$ followed by $|0\rangle \rightarrow |1\rangle$, $|-1\rangle \rightarrow |0\rangle$, and $|-2\rangle \rightarrow |-1\rangle$. Figure S2 in the Supporting Information shows the transition assignment with B parallel to the X, Y, and Z axes.

(17) Sometimes a different set of fourth-rank zfs terms is used,[22] comprised of parameters a and F. Parameter a represents cubic splitting, while F reflects the deviation from the cubic symmetry. The relations between two sets of spin Hamiltonian parameters are $a = 24B_4^4$ and $F = 36B_4^4 - 180B_4^0$. In cubic symmetry, $B_4^4 = 5B_4^0$; thus, $F = 0$.

(18) Abragam, A.; Bleaney, B. *Electron Paramagnetic Resonance of Transition Ions*; Dover Publications: New York, 1986.

(19) Wilkinson, J. H. *The Algebraic Eigenvalue Problem*; Clarendon: Oxford, England, 1965; p 290.

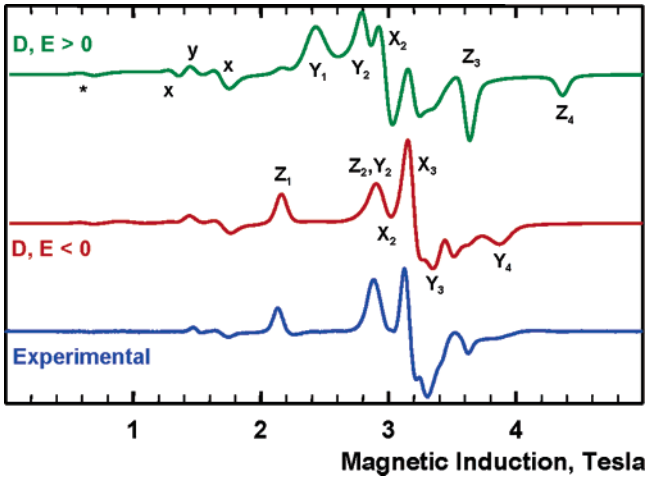

Figure 7. Experimental EPR spectrum of $[Cu_4(NH_3)_4(HL)_4][CdBr_4]Br_2 \cdot 3dmf \cdot H_2O$ at 4.0 K and 93.654 GHz (bottom) and spectra simulated with either $D = -0.3529$ cm^{-1} and $E = -0.0469$ cm^{-1} (center) or $D = +0.3529$ cm^{-1} and $E = +0.0469$ cm^{-1} (top). Boltzmann population of the M_S levels at low temperature affects the EPR resonance intensities, allowing determination of the sign of D. The sign of E depends on labeling of the X and Y axes if g_x and g_y are different and is irrelevant otherwise. Capital letters X, Y, and Z indicate the orientations of the magnetic field at which the respective "allowed" transitions occur, while small letters indicate the "forbidden" transitions. The transition labeled with an asterisk is an off-axial turning point with $\Theta = 90°$ and $\Phi = 45°$. Transition assignment and energy levels are shown in Figure S2 in the Supporting Information.

in the cubic copper tetramer $Cu_4OCl_6(TPPO)_4$[20] was explained exclusively in terms of $B_4^4 = 5B_4^0$, with $B_4^0 = 0.0044$ cm^{-1}, causing an overall zfs of ca. 0.53 cm^{-1}, while both D and E were equal to 0. The symmetry of our compound is lower; thus, vanishing D and E cannot be expected. The question of whether the fourth-rank terms $B_4^i\mathbf{O}_4^i$ should be taken into account is much more difficult. Typically, these terms were neglected in symmetries lower than cubic.[21] In our case, the calculated quartic parameters are found to be small and the estimated errors are comparable to their magnitudes. Single-crystal measurements need to be performed to determine them more definitively, but currently we do not have such possibilities in high-frequency EPR. Symmetry of the spectra indicates that there is no need to include the very rarely applied third-rank term $B\mathbf{S}^3$.[22] The sign of D is easily determined from the high-frequency spectra at low temperatures (Figure 7) because the combined zero-field and Zeeman interaction is not small compared to kT, which is the opposite of the situation encountered in standard low-frequency EPR (see also Figure 7 and Figures S1 and S2 in the Supporting Information). The g values that may appear surprising for copper(II) refer to the exchange-coupled system and seem to be justified by the tetramer structure. Although we do not know g values for separate copper atoms in the tetrameric complex, they are expected to be close to, if not the same as, those in the related compound $[Cu_2Zn_2(NH_3)_2Br_2(HL)_4]Br_2 \cdot CH_3OH$, in which the environment of copper is similar to that in the tetramer studied in this work. That complex exhibits very typical g values, $g_{x,y} = 2.052$ and $g_z = 2.250$,[23] but even in the absence of these data, one would estimate $g_{x,y} = 2.05$ and $g_z = 2.25$. The relationship between the tensors $\mathbf{g}_1$ through $\mathbf{g}_4$ of individual metal ions and the effective $\mathbf{g}$ tensor for the $S = 2$ state is[11,24]

$$\mathbf{g}_{S=2} = (\mathbf{g}_a + \mathbf{g}_b + \mathbf{g}_c + \mathbf{g}_d)/4 \qquad (12)$$

The systems of coordinates for each of the four $\mathbf{g}$ tensors were set up after averaging the positions of the disordered atoms. The g_z axis for each copper atom was assumed to be perpendicular to the least-squares plane of the four equatorial ligand atoms, while the g_x axis was in the plane containing the direction of g_z and the copper-bridging oxygen vector. The choice of the g_x and g_y directions is arbitrary in the plane perpendicular to g_z because g_x equals g_y. All four $\mathbf{g}$ tensors were transformed to a common system of coordinates, and the resulting $\mathbf{g}$ matrices were used to calculate $\mathbf{g}_{S=2}$ according to eq 12. The $\mathbf{g}_{S=2}$ matrix was finally diagonalized, resulting in $g_{xx} = 2.140$, $g_{yy} = 2.141$, and $g_{zz} = 2.072$. The agreement between the "expected" and experimental values seems to be excellent. (If the molecule were based on an undistorted cube, one would expect $g_{xx} = g_{yy} = 2.15$ and $g_{zz} = 2.05$.) The direction of g_{zz} for $S = 2$, as obtained from diagonalization, is perpendicular within 0.5° to two faces of the distorted Cu_4O_4 cube that are defined by the atoms Cu(2)−Cu(3)−O(3)−O(5) and Cu(1)−Cu(4)−O(1)−O(7), respectively.

Dipolar Contribution to the zfs Parameters. Formula (3) in ref 25 was used to calculate dipolar tensors for each of the six magnetic dipole−dipole interactions in the tetrameric system:

$$D_{\alpha\gamma} = g_{1\alpha}\{\sum_i g_{2i} d_{\gamma i}(d_{\alpha i} - 3\sigma_\alpha \sum_j d_{ji}\sigma_j)\}\mu_B^2/r^3 \qquad (13)$$

$g_{1\alpha}$ and g_{2i} are the $\mathbf{g}$ components for the two ions 1 and 2 in a pair, $d_{\gamma i}$ values are elements of the matrix that transforms $\mathbf{g}_2$ axes into $\mathbf{g}_1$ axes, and σ_α values are the direction cosines of the vector $\mathbf{r}$ joining atoms 1 and 2, expressed in the $\mathbf{g}$ axes of atom 1. All six tensors were then transformed into a common system of coordinates and added according to eq 14, which relates the zfs tensor components expressed in terms of the spins of separate ions and those appropriate for the total spin $S = 2$[11]

$$D_{ij}(S = 2) = \frac{1}{12}\sum_k D_{ij}^{(k)} \qquad (14)$$

where k runs over the six interactions a−b, b−c, c−d, a−d, a−c, and b−d.

Equation 13 results in a nonsymmetric tensor in the absence of the inversion center in an interacting pair.[25] The

(20) Black, T. D.; Rubins, R. S.; De, D. K. *J. Chem. Phys.* **1984**, *80*, 4620−4624.
(21) Bencini, A.; Gatteschi, D.; Zanchini, C.; Haasnoot, J. G.; Reedijk, J. *J. Am. Chem. Soc.* **1987**, *109*, 2926−2931.
(22) McGarvey, B. R. *Electron Spin Resonance of Transition Metal Complexes, Transition Metal Chemistry*; Marcel Dekker: New York, 1966; Vol. 3.
(23) To be published separately.
(24) Rubins, R. S.; Black, T. D.; Barak, J. *J. Chem. Phys.* **1986**, *85*, 3770−3775.
(25) Carr, S. G.; Smith, T. D.; Pilbrow, J. R. *J. Chem. Soc., Faraday Trans. 2* **1974**, *70*, 497−511.

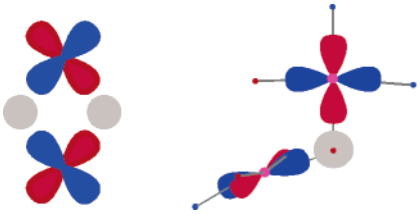

Figure 8. Arrangement of magnetic orbitals (x^2-y^2) in dimeric dibridged copper complexes (left) and in the tetramer studied in this work (right). Gray spheres represent the bridging oxygen atoms. A fragment of the tetramer structure with nitrogen (blue dots) and oxygen (red dots) atoms is also shown.

asymmetry in the resulting sum of tensors was not very pronounced, however, and because we are only trying to estimate the dipolar contribution, the off-diagonal tensor components i,j and j,i were replaced by their averages and the resulting symmetric matrix was diagonalized, yielding $D_{xx} = -0.012$ cm^{-1}, $D_{yy} = -0.0012$ cm^{-1}, and $D_{zz} = 0.014$ cm^{-1}. The direction of D_{zz} is 34° away from the direction of $g_{zz}(S = 2)$ found above.

Application of the relations between D, E, and the zfs tensor components

$$D = (2D_{zz} - D_{xx} - D_{yy})/2, \quad E = (D_{xx} - D_{yy})/2 \qquad (15)$$

finally yields $D_{\text{dipole}}(S = 2) = 0.02$ cm^{-1}. This is only about $^1/_{18}$ of D as determined from EPR and carries the opposite sign, indicating overwhelming contribution of the exchange interactions to the zfs in the tetranuclear molecule. Calculated $E_{\text{dipole}}(S = 2)$ is -0.005 cm^{-1}, 1 order of magnitude less than the experimental E value.

Discussion

Metal−Metal Interactions. Strong dependence of the exchange integral magnitude versus the Cu−O−Cu angle is well documented in dimeric dibridged complexes. The exchange interaction is ferromagnetic for the Cu−O−Cu angles less than 97° and antiferromagnetic for larger angles.[26] Our tetramer is decidedly ferromagnetic, however, despite the Cu−O−Cu angle magnitude of 107°. The arrangement of magnetic orbitals in the tetramer is very different from that in the dimers, and it is easy to see that the overlap of the x^2-y^2 orbitals in each pair of bridged copper ions is largely reduced compared to the situation in dimeric copper compounds (Figure 8). Only one lobe of the x^2-y^2 orbital of one ion is in a position to interact through the bridging atom with one lobe of the x^2-y^2 orbital of another ion. A decreased overlap magnitude favors the ferromagnetic character of metal−metal exchange interactions. The argument of the "orthogonality of bridging connections" was also used in ref 15 to explain the ferromagnetic interaction in a tetrameric copper system with even greater Cu−O−Cu angles, 139.2−140.5°. On the other hand, the tetramer in ref 9 is antiferromagnetic despite small bridging angles spanning the range 95.7−103.4°. Apparently, the structure-exchange-interaction relations for the dimeric complexes cannot be safely applied to the tetrameric systems, in accord with the foregoing discussion. The spin quintet is not very often the ground state in tetranuclear copper complexes.[13−15,27−29] Graham et al. recently discussed the structure-exchange-interaction correlations in tetranuclear copper compounds that, however, could be treated as pairs of noninteracting dimers.[30]

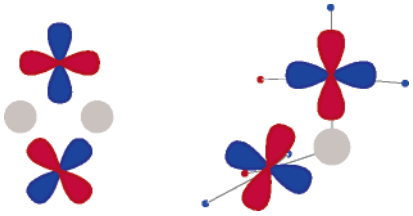

Figure 9. Arrangement of orbitals that are thought to contribute to the anisotropic exchange interactions in the binuclear dibridged compounds (left, orbitals x^2-y^2 and xy) and in the tetramer (right, orbitals x^2-y^2 and xz). Gray spheres represent the bridging oxygen atoms. In the tetramer, the x^2-y^2 orbital of each copper atom points approximately toward the equatorial nitrogen and oxygen atoms (shown in the tetramer structure fragment as blue and red dots, respectively). The Z axis of the upper-right copper atom is perpendicular to the paper plane, but the Z axis of the lower-left copper atom roughly lies in the paper plane.

Anisotropic Exchange and the zfs Parameters. It was proposed in the case of the binuclear dibridged copper complexes that the ferromagnetic exchange interaction between the ground state x^2-y^2 of one copper ion and the excited state xy of another copper ion (Figure 9) contributes a negative amount to the D_{zz} component of the zfs tensor **D**, while the D_{xx} and D_{yy} components of the anisotropic exchange were assumed to be negligible.[31−35] In that approach, D_{zz} has the same direction as g_{zz} and its magnitude is proportional to $(g_{zz} - 2.0023)^2 J(x^2-y^2,xy)$. Values of the exchange integral $J(x^2-y^2,xy)$ found from EPR for copper dimers[31−35] and for a vanadium dimer[35] were of the order of hundreds of wavenumbers. An analysis of the exchange contribution to the zfs was also attempted in the case of a carboxylato-bridged copper dimer.[36] The magnitude and the ferromagnetic character of the $J(x^2-y^2,xy)$ interaction were confirmed by studies on a rare heteronuclear vanadium−copper binuclear compound.[37] In the latter system, the exchange interaction

(26) Crawford, V. H.; Richardson, H. W.; Wasson, J. R.; Hodgson, D. J.; Hatfield, W. E. *Inorg. Chem.* **1976**, *15*, 2107−2110.
(27) Jones, D. H.; Sams, J. R.; Thompson, R. C. *Inorg. Chem.* **1983**, *22*, 1399−1401.
(28) Jezowska-Trzebiatowska, B.; Jezierska, J.; Baranowski, J.; Ozarowski, A. *J. Mol. Struct.* **1980**, *61*, 337−342.
(29) Sain, S.; Maji, T. K.; Mostafa, G.; Lu, T. H.; Ribas, J.; Tercero, X.; Chaudhuri, N. R. *Polyhedron* **2003**, *22*, 625−631.
(30) Graham, B.; Hearn, M. T. W.; Junk, P. C.; Kepert, C. M.; Mabbs, F. E.; Moubaraki, B.; Murray, K. S.; Spiccia, L. *Inorg. Chem.* **2001**, *40*, 1536−1543.
(31) Bencini, A.; Gatteschi, D. In *Magnetostructural Correlations in Exchange Coupled Systems*; Gatteschi, D., Kahn, O., Willett, R. D., Eds.; D. Reidel: Dordrecht, The Netherlands, 1985; p 241.
(32) Banci, L.; Bencini, A.; Gatteschi, D.; Zanchini, C. *J. Magn. Reson. (1962−1992)* **1982**, *48*, 9−19.
(33) Banci, L.; Bencini, A.; Gatteschi, D. *J. Am. Chem. Soc.* **1983**, *105*, 761−764.
(34) Bencini, A.; Gatteschi, D.; Zanchini, C. *Inorg. Chem.* **1985**, *24*, 700−703.
(35) Ozarowski, A.; Reinen, D. *Inorg. Chem.* **1986**, *25*, 1704−1708.
(36) Jezierska, J.; Glowiak, T.; Ozarowski, A.; Yablokov, Y. V.; Rzaczynska, Z. *Inorg. Chim. Acta* **1998**, *276*, 28−36.
(37) Kahn, O.; Tola, P.; Galy, J.; Coudanne, H. *J. Am. Chem. Soc.* **1978**, *100*, 3931−3933. Kahn, O.; Galy, J.; Jaud, J.; Morgenstern-Badarau, I. *J. Am. Chem. Soc.* **1982**, *104*, 2165−2176.

between the ground states of coupled ions, $J(x^2-y^2,xy)$ represents the isotropic exchange integral in the Hamiltonian $H = J\mathbf{S}_1\mathbf{S}_2$ and was found to be -118 cm^{-1} from the magnetic susceptibility measurements.[37] The model relating $J(x^2-y^2,xy)$ to the zfs parameter D has been criticized for its oversimplifications.[38] Application of even that oversimplified theory to a tetramer with lowered symmetry of individual metal−metal interactions is very difficult, and to our knowledge, it has never been attempted. In dimers, the directions of g components of two ions are parallel, thus providing a convenient coordinate frame for the zfs tensor. The largest component of the anisotropic exchange interaction is expected by theory and found experimentally along the direction of g_{zz}, although in some cases, deviations from that idealized picture have been observed.[39] In the tetramer, the Z_a and Z_b axes of bridged ions "a" and "b" are approximately perpendicular to each other (Figure 9). The interaction analogous to the (x^2-y^2, xy) in dimers is (x^2-y^2, xz) in the tetramer (Figure 9). Because of the lowered symmetry of the bridges, it is difficult to predict the ferro- or antiferromagnetic character of that interaction. $J(x^2-y^2,xy)$ is expected to have ferromagnetic character in dimers that is due to the zero overlap of the orbitals x^2-y^2 and xy of two ions. That overlap is zero in dimers because of the equality of the positive and negative contributions associated with the positive and negative lobes of the x^2-y^2 orbital in symmetric systems (Figure 9). In the tetramer under question, there is only one contribution to this overlap because there is only one bridging atom (Figure 9) and therefore the overlap cannot be equal to zero. Presumably, this may result in the reduced ferromagnetic or even antiferromagnetic exchange integral $J(x^2-y^2,xz)$. In addition, orbitals xy of each copper atom are in a position (although less advantageous than xz) to interact with x^2-y^2 orbitals of their partners in respective bridges and may contribute to the zfs. We will thus not try to relate particular orbital interactions to the spin Hamiltonian parameter D. Because the dipolar contribution to zfs is negligible (see above), it is possible to show that the exchange-related zfs tensors for individual copper−copper interactions cannot be axial. The zfs tensor $\mathbf{D}_{S=2}$ is a sum of the zfs tensors for each of the interacting copper pairs, a−b, b−c, c−d, and d−a according to eq 14. The orientation and elements of these tensors are not experimentally available, but we may expect that all four tensors are equal except for being oriented differently in space according to the molecular geometry. The zfs tensor for an interaction a−b is likely to be diagonal in a system of coordinates[40,41] in that local axis **1** is perpendicular to the plane $Cu_a-O_{bridge}-Cu_b$, local axis **2** dissects the $Cu_a-O_{bridge}-Cu_b$ angle, and axis **3** is perpendicular to both **1** and **2**. Local coordinates for the other three interactions, b−c, c−d, and d−a, are set up in the same way. It is interesting to note here that the four bridge planes are either nearly parallel or nearly perpendicular to one another. Using the atom numbering scheme from the X-ray structure (Figures 1 and 2), we have the following angles between the planes: Cu(1)O(1)Cu(3)−Cu(3)O(3)Cu(4) = 90.4°, Cu(1)O(1)Cu(3)−Cu(4)O(7)Cu(2) = 1.6°, Cu(1)O(1)Cu(3)−Cu(2)O(5)Cu(1) = 89.5°, Cu(3)O(3)Cu(4)−Cu(4)O(7)Cu(2) = 90.4°, Cu(3)O(3)Cu(4)−Cu(2)O(5)Cu(1) = 2.4°, and Cu(4)O(7)Cu(2)−Cu(2)O(5)Cu(1) = 89.6°. Each of the four zfs tensors has the same unknown quantities (x, y, z) on its diagonal. If the tensor is also assumed to be axial, like (x, x, z), which in EPR is equivalent to (0, 0, $z - x$),[42] then there is only one unknown number $u = z - x$; therefore, the tensor diagonal has either form (u, 0, 0), (0, u, 0), or (0, 0, u) because we do not know which one is the distinguished axis. Each tensor was rotated to a common system of coordinates, and eq 14 was applied to calculate the tensor components expressed in the total spin $S = 2$. After diagonalization of the resulting matrix and the application of eq 15, one obtains relationships between u and D and E of the spin Hamiltonian (eq 11). In the three cases above [(u, 0, 0), (0, u, 0), and (0, 0, u)], we find $D = -0.166u$, $E = 0$; $D = 0.133u$, $E = 0.0005u$; and $D = 0.033u$, $E = -0.001u$, respectively. In each case, D_{zz} for $S = 2$ deviates by less than 1° from the direction of $g_{zz}(S = 2)$. Thus, it is clear that the tensors of individual metal−metal interactions cannot be axial because no E of suffcient size is generated to reproduce the experimental E/D ratio of 0.13.

Failure To Observe Spectra of the Excited Triplet States. The fact that no triplet-state spectra were observed, even at elevated temperatures at which point the triplet states (see Figure 3 and Figure S4 in the Supporting Information) are substantially populated, requires comment. Spectra due to thermally accessible excited states have often been observed in polynuclear compounds,[11,14,20,21,24,30,33−36,40,41,43,44] and spectral intensity measurements occasionally served to help in the determination of the exchange integrals. Sometimes, however, such excited-state spectra are not observed even if these states are populated. In binuclear oxygen-bridged iron(III) complexes, the first excited state, $S = 1$, is not observed in X- or Q-band EPR, while the higher excited states $S = 2$ and 3 are observed.[40,41] In that case, very high zfs parameters expected for $S = 1$ explain the absence of the triplet-state spectra. Most relevant to the present work is the absence of triplet-state spectra in other tetrameric copper compounds. Because of the high symmetry of the copper tetramer $Cu_4OCl_6(TPPO)_4$, all three triplet states are degenerate.[20,24] It was assumed that fast relaxation (presumably) within these three triplets may be responsible for the fact that only $S = 2$ was observed in EPR. The triazolato-bridged copper tetramer[11,21] is antiferromagnetic, with the energy

(38) Gribnau, M. C. M.; Keijzers, C. P. *Inorg. Chem.* **1987**, *26*, 3413−3414.
(39) Bencini, A.; Gatteschi, D.; Zanchini, C. *Inorg. Chem.* **1986**, *25*, 2211−2214.
(40) Ozarowski, A.; McGarvey, B. R.; Drake, J. E. *Inorg. Chem.* **1995**, *34*, 5558−5566.
(41) Holgate, S. J.; Bondarenko, G.; Collison, D.; Mabbs, F. E. *Inorg. Chem.* **1999**, *38*, 2380−2385.
(42) The effect on EPR of a diagonal zfs tensor with the diagonal components (x, y, z) is the same as that of a tensor ($x + c$, $y + c$, $z + c$), where c is an arbitrary number.
(43) Khangulov, S. V.; Pessiki, P. J.; Barynin, V. V.; Ash, D. E.; Dismukes, D. C. *Biochemistry* **1995**, *34*, 2015−2025.
(44) Howard, T.; Telser, J.; DeRose, V. J. *Inorg. Chem.* **2000**, *39*, 3379−3385.

level scheme inverted as compared to Figure 3. The spectrum of the lowest excited triplet, labeled[11,45] $|111\rangle$, that is located 12 cm^{-1} above the singlet ground state was observed only at very low temperatures, but no resonances attributable to the other two degenerate triplets $|101\rangle$ and $|011\rangle$ appeared, even at the temperatures at which these triplets are populated. Line broadening by fast relaxation was again invoked[11] to explain their absence. In our case, the lone triplet state $|111\rangle$ (Figure 3) is highly excited and not populated at low temperatures. The two lower-energy triplets, $|101\rangle$ and $|011\rangle$, are degenerate and, in addition, they are very close to one of the $S = 0$ states, $|000\rangle$. This situation may lead to enhanced relaxation, as was suspected before,[11,20,21,24] and cause broadening of the resonance lines.

Magnitude of D in Triplet States. Relations between the components of the zfs tensors of six individual interactions and those for the $S = 2$ ($|112\rangle$) and $S = 1$ states[11,21] are in the matrix notation

$$\mathbf{D}_{S=2} = (\mathbf{D}_{ab} + \mathbf{D}_{bc} + \mathbf{D}_{cd} + \mathbf{D}_{da} + \mathbf{D}_{ac} + \mathbf{D}_{bd})/12 \quad (16a)$$

$$\mathbf{D}_{S=1(|111\rangle)} = (\mathbf{D}_{ab} + \mathbf{D}_{bc} + \mathbf{D}_{cd} + \mathbf{D}_{da} - \mathbf{D}_{ac} - \mathbf{D}_{bd})/4^{46} \quad (16b)$$

$$\mathbf{D}_{S=1(|101\rangle)} = \mathbf{D}_{ac}/2, \quad \mathbf{D}_{S=1(|011\rangle)} = \mathbf{D}_{bd}/2 \quad (16c)$$

The $S = 1$ state in eq 16b is the high-energy lone triplet in Figure 3, while eq 16a is equivalent to eq 14. Because bridges Cu_a-O-Cu_c and Cu_b-O-Cu_d are weak, we may expect that interactions $\mathbf{D}_{ac}$ and $\mathbf{D}_{bd}$ do not contribute much to the **D** tensors in either the $S = 2$ or $S = 1$ states. Then, we have $\mathbf{D}_{S=1} = 3\mathbf{D}_{S=2}$ for the lone triplet $|111\rangle$ and essentially no zfs in the degenerate pair of triplets. The experimental ratio of $\mathbf{D}_{|111\rangle}/\mathbf{D}_{S=2}$ in another tetrameric system[11,21] is 2.39. The g values in triplet $|111\rangle$ should be the same as those for the quintet, but in states $|101\rangle$ and $|011\rangle$, they should be close to the g values of a single copper ion[47] (formulas 4.83−4.86 in ref 11). The spectrum of the lone triplet $|111\rangle$ could overlap with the quintet spectrum, as the outermost resonances in a triplet spectrum appear at the magnetic fields

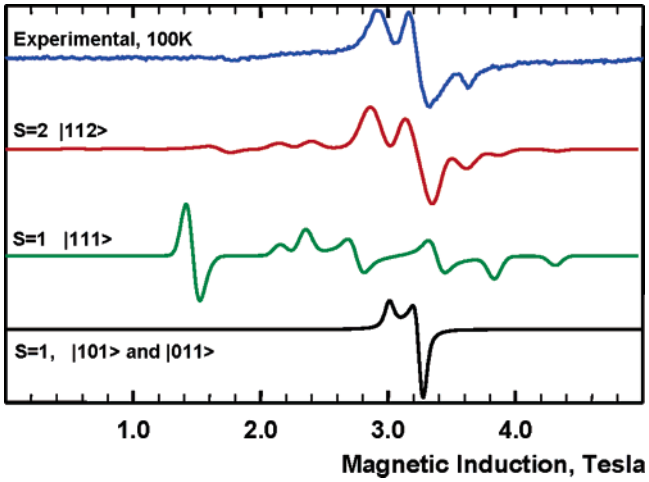

Figure 10. Experimental and simulated spectra at 100 K and 93.654 GHz. The $S = 2$ spectrum was simulated with the spin Hamiltonian parameters as found at 15 K. The hypothetical spectrum of the triplet $|111\rangle$[45] was simulated with **g** components equal to those of the quintet spectrum,[47] while D and E were assumed to be 3 times larger than those of the quintet. In simulation of the spectra that were due to the triplets $|101\rangle$ and $|011\rangle$, $D = 0$, $E = 0$, $g_x = 2.05$, $g_y = 2.07$, and $g_z = 2.23$ were used.[47]

($h\nu \pm D_{S=1}$)/$g_z\mu_B$, while in the quintet, one finds ($h\nu \pm 3D_{S=2}$)/$g_z\mu_B$ and $D_{S=1} = 3D_{S=2}$ (here D is the parameter of the spin Hamiltonian (eq 11), while boldfaced **D** denotes the zfs tensors). Figure 10 shows the hypothetical triplet spectra simulated at 100 K with the above assumptions. In summary, even if the triplets do contribute at higher temperatures, their spectra may largely overlap with the quintet spectrum. Single-crystal experiments that we are planning for the future may be the only way to detect these spectra or to definitively prove their absence.

Acknowledgment. This work was supported by the INTAS (Project 03-51-4532) and by the NHMFL (Project 7300-034). The NHMFL is funded by the NSF through the Cooperative Agreement No. DMR-0084173 and the State of Florida.

Supporting Information Available: (1) CIF file containing crystallographic data for $[Cu_4(NH_3)_4(HL)_4][CdBr_4]Br_2 \cdot 3dmf \cdot H_2O$. (2) Figure S1: EPR spectra taken at various temperatures. (3) Figure S2: energy levels of the quintet state with the magnetic field parallel to either the X, Y, or Z axis, as well as the experimental and simulated EPR spectra with resonance assignment. (4) Figure S3: the $[Cu_4(NH_3)_4(HL)_4]^{4+}$ cation viewed along the $\mathbf{g}_{S=2}$ tensor axes. (5) Figure S4: relative intensities of EPR transitions within the quintet and triplet states. (6) Table of the magnetic susceptibilities. This material is available free of charge via the Internet at http://pubs.acs.org.

IC049044P

(45) The total spin of a tetramer, $\mathbf{S}_T = \mathbf{S}_a + \mathbf{S}_b + \mathbf{S}_c + \mathbf{S}_d$, is built up[11,21] in two stages, $\mathbf{S}' = \mathbf{S}_a + \mathbf{S}_c$, $\mathbf{S}'' = \mathbf{S}_b + \mathbf{S}_d$, and $\mathbf{S}_T = \mathbf{S}' + \mathbf{S}''$. The states are then labeled as $|\mathbf{S}'\mathbf{S}''\mathbf{S}_T\rangle$.

(46) Note that formula (4.86) in ref 11 should read $\mathbf{D}_{111} = (-\mathbf{D}_{12} + \mathbf{D}_{13} + \mathbf{D}_{14} + \mathbf{D}_{23} + \mathbf{D}_{24} - \mathbf{D}_{34})/4$ instead of $\mathbf{D}_{111} = (-\mathbf{D}_{12} + \mathbf{D}_{13} + \mathbf{D}_{14} + \mathbf{D}_{23} + \mathbf{D}_{24} - \mathbf{D}_{34})$. That formula is reported properly in ref 21 with a different numbering scheme.

(47) The **g** tensors in triplet states $|101\rangle$ and $|011\rangle$ are $(\mathbf{g}_a + \mathbf{g}_c)/2$ and $(\mathbf{g}_b + \mathbf{g}_d)/2$, respectively. The $\mathbf{g}_{zz}$ tensor axis of Cu_a is approximately 30° away from that of Cu_c, with a similar relation between the Cu_b and Cu_d axes. In both the quintet and triplet $|111\rangle$, the **g** tensor is calculated from eq 12.